AMSE JOURNALS-AMSE IIETA publication-2017-Series: Advances C; Vol. 72; N°3; pp 181-202
Submitted Oct. 18, 2017; Revised Dec. 26, 2017; Accepted Dec. 26, 2017
https://doi.org/10.18280/ama_c.720301

Fault Eccentricity Diagnosis in Variable Speed Induction Motor Drive Using DWT

* Rouaibia Reda[1], **Arbaoui fayçal[2], ***Bahi Tahar[3]
*Faculty of Sciences and Technology University Mohamed-Cherif Messaadia LEER Lab
Souk Ahras, Algeria. (rouaibia.reda@hotmail.com)
** Department of Electronics Engineering Badji Mokhtar University LASA Lab
Annaba, Algeria. (arbaoui@univ-annaba.org)
***Department of Electrical Engineering Badji Mokhtar University LASA Lab
Annaba, Algeria. (tbahi@hotmail.fr)

Abstract

This paper describes the monitoring and diagnosis of eccentricity fault in variable speed induction motor drive. The used control technique is the indirect field oriented control (IFOC) fuzzy logic based controller to ensure the robust speed regulation and to compensate the fault effects. The variable speed induction motor can be affected by various kinds of faults. Airgap eccentricity is one of the major defects occurring in such electric drives; its detection could be useful for preventing potential catastrophic failures. A dynamic model taking into account the faults is proposed based on the approach of magnetically coupled coils to simulate the behavior of eccentricity faults in induction motor. This work presents two approaches for diagnosis and detection of eccentricity faults and evaluation of their severity based on monitoring of the stator current signals, using Park vector method and discrete wavelet transform (DWT) with different approaches to distinguish healthy as well as faulty conditions of the machine. The obtained simulation results via the proposed technique allow detection and diagnosis of eccentricity fault and identify their severity.

Key words

Fuzzy logic controller, Diagnosis, Induction motor, Mixed eccentricity, Discrete wavelet transform.

1. Introduction

Nowadays induction machine (IM), in particular, squirrel cage IM is the most used one in industries requiring high performance. Furthermore, industrial applications widely needs to variable speed IM. However, controlling these electric drives present some difficulties due to their complex and non-linear behaviors during saturation effect and due to their highly coupled structure between flux and torque.We can get around these limitations by the use of field oriented control theory (FOC) [1].This technique referred as vector control, induced large changes in the field of electrical drives.The FOC schemes require the closed control of flux and torque current (inner loop) and speed control (outer loop).This structure is divided into two groups: the indirect field oriented control (IFOC) proposed by Hasse [2] and the direct field oriented control (DFOC) proposed by Blashke [3].

For several decades, traditional vector control using conventional PI controller were applied to power electronics area and to control electric machines. Although conventional PI controllers showed simplicity in design and stability in performance, they are sensitive to load disturbances, parameter variation and require an accurate mathematical model of IM. To overcome the above problems, an intelligent controller based on fuzzy logic controller (FLC) is being used to enhance the performance of IM drives.

However, the control performance of IM is still influenced by uncertainties failures and faults due to production processes or operating conditions [4, 5]. Most of the faults occurring in the three-phase IM are due to change in the air-gap eccentricity.

Several methods have been developed for the identification of this kind of faults, originally based on electrical monitoring such as stator current monitoring [6], axial flux, instantaneous power [7], active reactive power, air-gap torque monitoring and current Park components [8] followed by thermal and vibration monitoring [9]. Several authors applied modern computing approaches such as genetic algorithm, wavelet analysis, expert systems, Neural Networks [10, 11], and Fuzzy Logic [12]. Others propose solutions based on the on-line condition monitoring method which is applied to heavy process industries [13].

In this work, we present two methods for detection and isolation of the eccentricity faults in a three-phase variable speed squirrel cage induction motor using an indirect field oriented control (IFOC) using a fuzzy logic based speed controller in order to maintain good performances in degraded mode, that is, in the presence of eccentricity defects.The first method is based on fault detection with the evolution of components i_{ds} and i_{qs} currents in the plan of Park. The second method is based on discrete wavelet decomposition (DWT) [14-16].

The paper is organized as follows; first we presented a brief overview of the induction machine dynamic model and the function of the vector controlled drive. Then, the methodology of the fuzzy logic controllers is presented. The application of the Park's vector approach and wavelet analysis DWT as diagnostic methods, for early faults detection and for severity evaluation is investigated. A comparison of the IFOC simulation results between the eccentricity fault and healthy case are presented and discussed. Finally, conclusions are presented in the last section.

2. Dynamical Equations of the Induction Motor

The proposed model is based on a three-phase IM. The cage rotor model consists of *nb* identical and equally spaced bars shorted together by two identical end rings as shown in Fig.1.

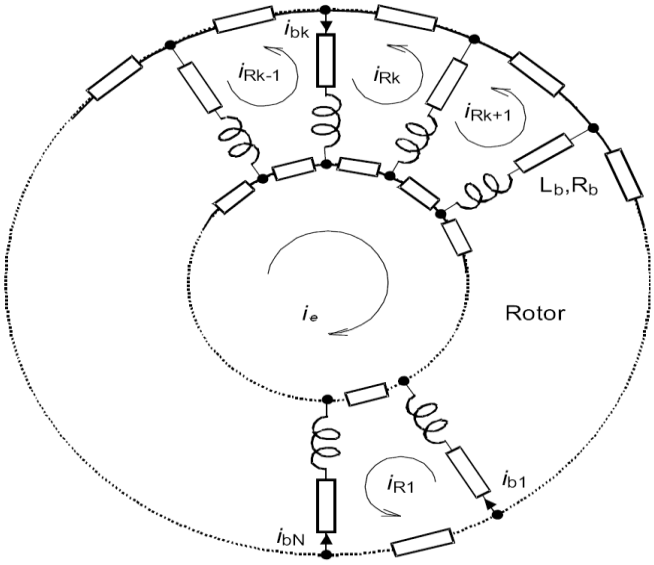

Fig.1. Equivalent Rotor mesh circuit

This approach offers a compromise in terms of model accuracy and computation time. In addition to that, this type of model can take into account several electromagnetic faults such as broken bars and eccentricity faults. The Model of the three-phase induction motor is presented by the system of equation:

$$[V] = [[R] + \frac{d[L]}{dt}][I] + [L]\frac{d[I]}{dt} \quad (1)$$

Which leads to

$$\frac{d[I]}{dt}=[L]^{-1}[[V]-[[R]+\frac{d[L]}{dt}]][I] \tag{2}$$

$$\frac{d[I]}{dt}=\begin{bmatrix}[L_s] & [L_{sr}]\\ [L_{sr}]^T & [L_r]\end{bmatrix}^{-1}.\left[[V]-\begin{bmatrix}[R_s] & \frac{d[L_{sr}]}{dt}\\ \frac{d[L_{sr}]^T}{dt} & [R_r]\end{bmatrix}\right].[I] \tag{3}$$

$$\begin{cases}[V]=[[V_s],[V_r]]^T\\ [Vs]=[V_{s1} \quad V_{s2} \quad V_{s3}]^T\\ [V_r]=[0 \quad 0 \quad 0 \quad \dots \quad 0]^T{}_{1\times nb+1}\end{cases} \tag{4}$$

$$\begin{cases}[I]=[[I_s],[I_r]]^T\\ [Is]=[I_{s1} \quad I_{s2} \quad I_{s3}]^T\\ [I_r]=[I_{r1} \quad I_{r2} \quad I_{r3} \quad \dots \quad I_{rnb} \quad I_e]^T{}_{1\times nb+1}\end{cases} \tag{5}$$

The stator resistance and inductance matrixes are (3x3):

$$[Rs]=\begin{bmatrix}r_s & 0 & 0\\ 0 & r_s & 0\\ 0 & 0 & r_s\end{bmatrix} \tag{6}$$

$$[Ls]=\begin{bmatrix}L_{s1p} & L_{s1s2} & L_{s1s3}\\ L_{s2s1} & L_{s2p} & L_{s2s3}\\ L_{s3s1} & L_{s3s2} & L_{3p}\end{bmatrix} \tag{7}$$

The principal inductance of the magnetizing stator phase is [4]:

$$L_{sp}=\frac{4\mu_0}{\pi.e.p^2}N_s{}^2LR \tag{8}$$

The total cyclic inductance of a stator phase is equal to the sum of the magnetizing and leakage inductances:

$$L_{sip}=L_{sp}+L_f \tag{9}$$

The mutual inductance between *i* and *j* stator phases is given as:

$$L_{sisj} = \frac{-L_{sp}}{2} \tag{10}$$

The rotor resistance and inductance matrixes are (nb+1) x (nb+1):

$$[R_r] = \begin{bmatrix} 2(R_r + R_e) & -R_b & 0 & \cdots & 0 & -R_b & -R_e \\ -R_b & 2(R_r + R_e) & -R_b & 0 & \cdots & 0 & -R_e \\ \ddots & \ddots & \ddots & \ddots & \ddots & \ddots & \vdots \\ \ddots & \ddots & \ddots & \ddots & \ddots & \ddots & \vdots \\ \ddots & \ddots & \ddots & \ddots & \ddots & \ddots & \vdots \\ -R_b & 0 & \cdots & 0 & -R_b & 2(R_r + R_e) & -R_e \\ -R_e & -R_e & \cdots & \cdots & \cdots & -R_e & nb.R_e \end{bmatrix} \tag{11}$$

$$[L_r] = \begin{bmatrix} L_{r1p} & L_{r1r2} & \cdots & \cdots & L_{r1r_{Nb}} & L_e \\ L_{r2r1} & L_{r2p} & \cdots & \cdots & L_{r2r_{Nb}} & L_e \\ \vdots & \vdots & \vdots & \vdots & \vdots & \vdots \\ \vdots & \vdots & \vdots & \vdots & \vdots & \vdots \\ L_{r_{Nb}r1} & L_{r_{Nb}r2} & \cdots & \cdots & L_{r_{Nb}r_{Nb}} & L_e \\ L_e & L_e & \cdots & \cdots & L_e & nb.L_e \end{bmatrix} \tag{12}$$

Where the principal inductance of a rotor mesh can be calculated by:

$$L_{rp} = \frac{N_r - 1}{N_r^2} \frac{\mu_0}{g} 2\pi LR \tag{13}$$

Therefore, the total inductance of rotor meshes *i:*

$$L_{rip} = L_{rp} + 2L_b + 2L_e \tag{14}$$

The mutual inductance between non-adjacent rotor meshes *i* and *j* is defined by:

$$\begin{cases} L_{rirj} = L_{rr-L_b} \\ L_{rr} = -\frac{1}{N_r^2} \frac{\mu_0}{g} 2\pi LR \end{cases} \tag{15}$$

The mutual inductance matrix between stator phases and rotor mesh is (*m* x *nb+1*)

$$[L_{sr}] = \begin{bmatrix} l_{s1r1} & l_{s1r2} & \cdots & \cdots & l_{s1r_{nb}} & 0 \\ l_{s2r1} & l_{s2r2} & \cdots & \cdots & l_{s2r_{nb}} & 0 \\ l_{s3r1} & l_{s3r2} & \cdots & \cdots & l_{s3r_{nb}} & 0 \end{bmatrix} \quad (16)$$

The mutual induction between the stator phase *m* and rotor mesh *k* is given by:

$$M_{smrk} = -M_{sr} \cos(p\theta - m\frac{2\pi}{3} + ka) \quad (17)$$

These electrical equations must be added to the following mechanical equation:

$$\frac{d\omega}{dt} = \frac{1}{J}(T_e - T_l + f_v.\omega) \quad \text{with} \quad \omega = \frac{d\theta}{dt} \quad (18)$$

The expression of electromagnetic torque *Te* is ultimately determined by the relationship below [4]:

$$T_e = \frac{1}{2}\begin{bmatrix}[I_s] \\ [I_r]\end{bmatrix}^T \frac{d}{d\theta}\begin{bmatrix}[L_s] & [L_{sr}] \\ [L_{rs}] & [L_r]\end{bmatrix}\begin{bmatrix}[I_s] \\ [I_r]\end{bmatrix} \quad (19)$$

3. Indirect Field Oriented Control

The most important aspect of field-oriented control applied to IM is the decoupling of stator current into two components, used for generating magnetizing flux and torque [1]. The decoupling allows us to control the IM as a simple DC machine with separate excitation [6]. The IFOC technique has simple implementation and is more reliable what makes it widely used in industry. To achieve field orientation along the rotor flux, the direct flux component is aligned in the direction of rotor flux φ_r.

$\varphi_{rq}=0$; $\varphi_{rd}=\varphi_r$, $V_{rd}=0$ and $V_{rq}=0$. (20)

The advantage of using a reference related to the rotating field frame is to have constant magnitudes. It's then easier to make the regulation, by acting on the i_{ds} and i_{qs} variables. The magnitudes φ_r and T_e are ordered separately. This results in:

$$\varphi_r = \frac{M_{sr}.i_{ds}}{1 + pT_r}; \quad (21)$$

$$\omega_{sl} = \frac{M_{sr}.i_{qs}}{T_r.\varphi_r} \tag{22}$$

$$T_e = \frac{p.M_{sr}.i_{qs}.\varphi_r}{L_r} = K.i_{qs} \tag{23}$$

Where ω_{sl}: is a slip frequency.

Hence, the analogy with DC machine performance is clearly established, by keeping the flux constant. The electric torque is found proportional to the i_{qs} component, and the flux φ_r and i_{ds} component of current can be related to the first-order linear transfer function where T_r is a rotor time constant. Fig.2. shows the block diagram of indirect field oriented control of 3-phases IM with a fuzzy logic based speed controller.

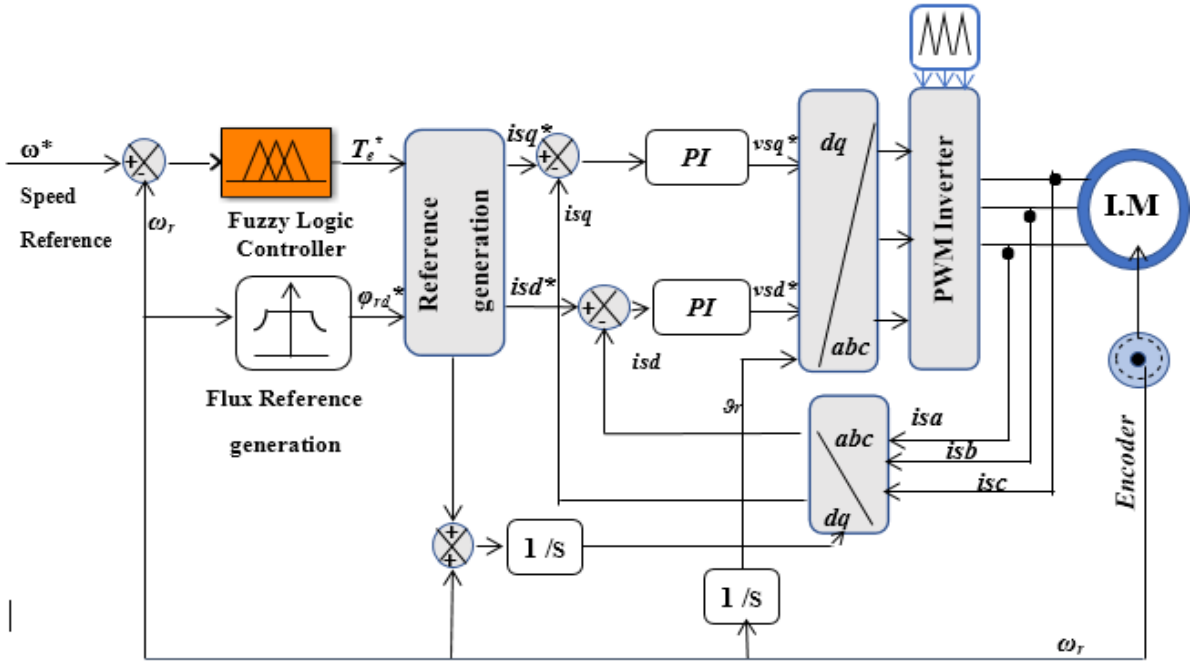

Fig. 2. Indirect field oriented control (IFOC) block diagram

4. Fuzzy Logic Controller

Fuzzy logic control (FLC) is a linguistic approach which attempt to imitate human control strategies in technical environments built from the use "if–then" rules provided by human experts that completely define the behaviour of the system. The FLC block diagram is shown in Fig 3.

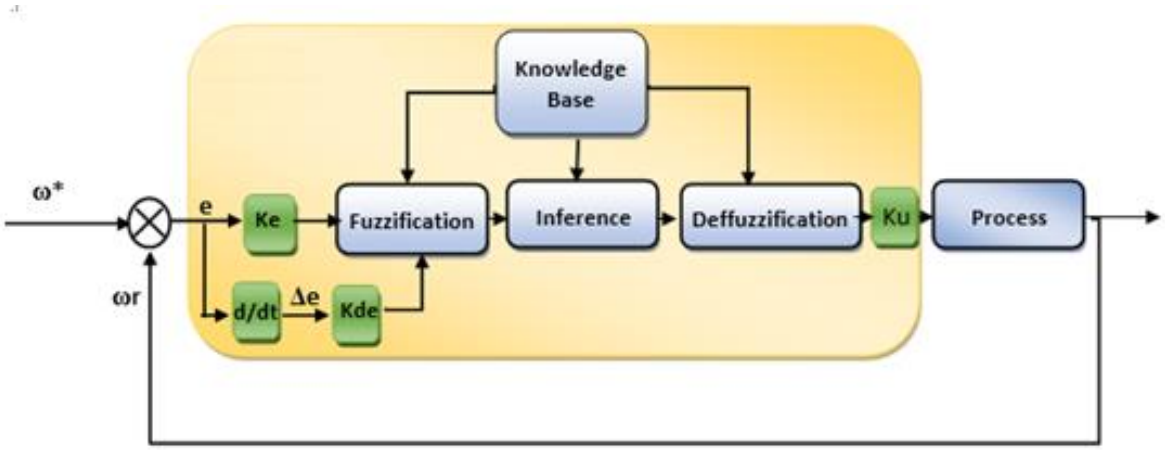

Fig.3. Fuzzy control bloc diagram

It is composed of four major blocks: fuzzification, knowledge base, inference engine, and defuzzification. There are two inputs, the first one is speed error *e(k)*, the second is the change of speed error *Δe(k)*. The output is the torque reference, calculated at every sampling time '*k*'

$$e(k) = w^*(k) - wr(k) \tag{24}$$

$$\Delta e(k) = e(k) - e(k-1) \tag{25}$$

Where e(k) is the error value, *ω*(k)* denotes the reference speed, *ωr(k)* is the actual speed and *Δe(k)* is the change of error at sampling time.

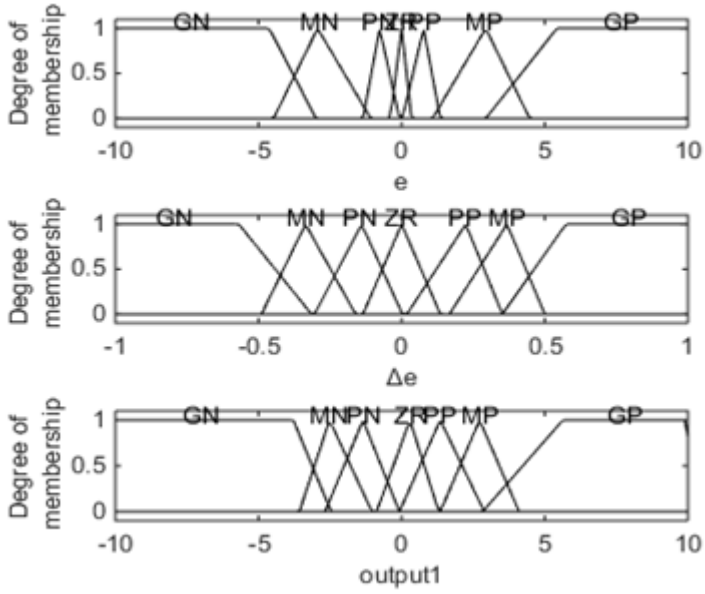

Fig4. Membership functions of the fuzzy logic controller for the error (e), the change of error (Δe), and the output (Δu)

Membership functions for input and output variables were normalized with values varying between [0-1], and associated with the following linguistic variables NB (Negative Big),NM(Negative Medium), NS(Negative Small), ZE(Zero Equal); PS(Positive Small), PM(Positive Medium) and PB(Positive Big) shown in Fig 4.

Each of the inputs and output–are processed by the inference mechanism that executes 7x7=49 rules summarized in Table1:

Table1. Rules base for the fuzzy controller

Δe\e	NB	NM	NS	ZE	PS	PM	PB
NB	NB	NB	NB	NB	NM	NS	ZE
NM	NB	NB	NB	NM	NS	ZE	PS
NS	NB	NB	NM	NS	ZE	PS	PM
ZE	NB	NM	NS	ZE	PS	PM	PB
PS	NM	NS	ZE	PS	PM	PB	PB
PM	NS	ZE	PS	PM	PB	PB	PB
PB	ZE	PS	PM	PB	PB	PB	PB

5. Eccentricity Fault Model

Eccentricity fault is more related with internal faults of the machine; it appears when there is an unequal air gap between rotor and stator. Three kinds of eccentricity can be considered: static eccentricity [4], dynamic eccentricity [23] and mixed eccentricity [18, 19]. In static eccentricity case (SE), the air gap becomes irregular; therefore, the minimum air gap location appears at a specific fixed position. Its function takes sinusoidal form with the angular position of the stator. Dynamic eccentricity (DE) exists when the axis of rotation coincides with the axis of stator but not with the axis of the rotor.The minimum air gap location then changes with the rotor's angular position and revolves with it. For the mixed eccentricity (ME), the two defects (SE) and (DE) are present at the same time and the axis of rotation is different from both axes of stator and rotor. In this work, we choose to study mixed eccentricity fault. The expression of the air gap that reflects this type of defect is expressed by the following equation:

$$e(\theta_s, \theta_r) = e + \varepsilon_s \cos(\theta_s) + \varepsilon_d \cos(\theta_s - \theta_r) \quad (26)$$

with

e: air gap of the machine;

$\varepsilon_s = a_1.e:$ percentage of static eccentricity;

$\varepsilon_d = a_2.e:$ percentage of dynamic eccentricity.

The fault frequency components of the eccentricity defect are based on expressions [19]:

$$f_{ecc} = f_s\left(1 \pm k\left(\frac{1-s}{p}\right)\right) \tag{27}$$

with

f_{ecc}: eccentricity fault frequency, f_s *:*fundamental frequency,

k = 0, 1, 2…n: is a constant and *s: is* the motor slip.

6. Fault Detection Methods

6.1 Park's Vector Approach

Park's vector approach is an easy way to decide if the machine is healthy or not. It means that the phase currents (i_{sa}, i_{sb}, i_{sc}) are to be transformed into a two-coordinate system with perpendicular axes (i_d, i_q) and placed on d-axis and q-axis respectively. In other words, transforming a three-dimensional system into a two-dimensional *(2-D)* [20].The current park vector components are functions of mains phase variables which are*:*

$$\begin{cases} i_d = \sqrt{\frac{2}{3}}(i_{sa}) - \frac{1}{\sqrt{6}}(i_{sb}) - \frac{1}{\sqrt{6}}(i_{sc}) \\ i_q = \frac{1}{\sqrt{2}}(i_{sb}) - \frac{1}{\sqrt{2}}(i_{sc}) \end{cases} \tag{28}$$

6.2 Wavelet Transform

The wavelet transform was introduced with the idea of overcoming the drawbacks of the Fourier transform. The wavelet transform assures both time-frequency analysis and time scale analysis with multi-resolution characteristic. The continuous wavelet transforms (CWT) is defined by the following equation

$$\psi_{s,\tau}(t) = \frac{1}{\sqrt{s}}\psi\left(\frac{t-\tau}{s}\right) \tag{29}$$

The parameter τ indicates the translation in time, and s is a scale parameter, $\psi(t)$ is the transforming function, also known as the mother wavelet.

The translation and the expansion transform the signal into another timescale. The representation form with smaller scales corresponds to the high-frequency components [21].

In the case of the DWT, the expansion and translation parameters s and τ are limited only to discrete values leading to the following expression:

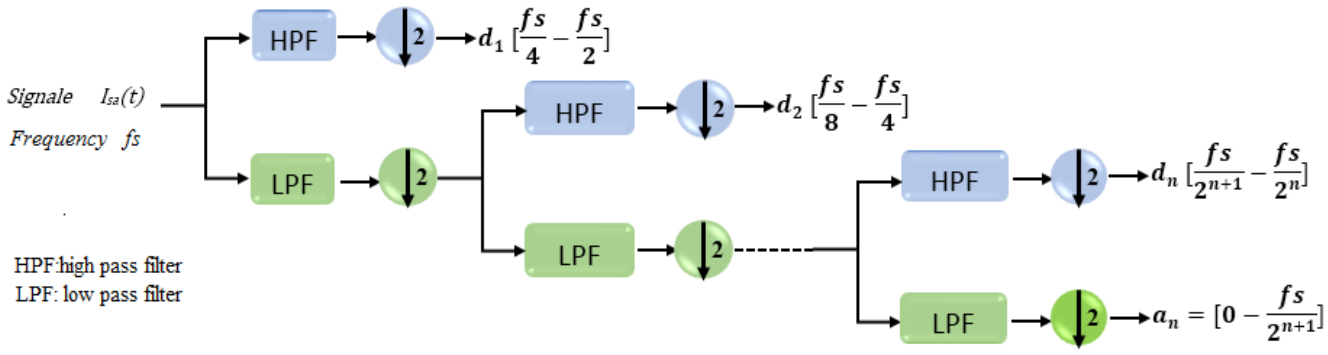

Fig.5. The DWT decomposition signal

$$\psi_{s,\tau}(t) = \frac{1}{\sqrt{s_0^j}}\psi\left(\frac{t - k\tau_0 s_0^j}{s_0^j}\right) \tag{30}$$

Where the whole numbers s and τ control the wavelets expansion and translation, respectively. For practical reasons, the simplest and most efficient discretization comes by choosing $s_0 = 2$ and $\tau_o = 1$:

$$\psi_{s,\tau}(t) = \frac{1}{\sqrt{2^j}}\psi\left(\frac{t - k2^j}{2^j}\right) = 2^{\frac{-j}{2}}\psi(2^{-j}t - k) \tag{31}$$

A signal $i_{sa}(t)$ can be decomposed and reconstructed by means of two components: approximation (a_j) and detail (d_j), where approximation can be interpreted as a high-pass filter (HPF) and detail as a low-pass filter (LPF) as shown in Fig 5.

This means that the approximation contains the low-frequency information of the original signal belonging to the interval $[0, fs/2^{(j+1)}]$ and detail contains the high-frequency information whose frequencies are included in the interval $[fs/2^{(j+1)}, fs/2^{(j)}]$.

Decomposition which uses discrete wavelet transform (DWT) of a signal is carried by a successive operation using (HPF) and (LPF) of the time domain signal. The reconstructed signal $i_{sa}(t)$ can be approximated using the DWT by [19-21]:

$$i_{sa}(t) = d_1 + d_2 + ... + d_n + a_n \tag{32}$$

6.3 Wavelet Energy

The fault diagnosis is based on observation and comparison between the energy associated to each level of signal decomposition. The stator current signal contains information included in each frequency band which is resulting from the wavelet packet decomposition. The energy value for each frequency band is defined by [10], [15]:

$$E_j = \sum_{k=1}^{n} D^2{}_{j,k}(n) \tag{33}$$

Where j: is the level of detail and D_{jk} is the detail signal at level j and n is the total number of samples of the signal.

The energy values of decomposition levels contain necessary diagnostic information. The plot of these values can be used to diagnose faults in the squirrel cage IM and it can also assess the severity degree of the fault. Before the calculation of the wavelet energy, the number of the decomposition levels must be well defined by the following relationship [16] [21, 22]:

$$N = \text{int}\left[\frac{\log(\frac{f_e}{f_s})}{\log(2)}\right] + 2 \tag{34}$$

With fs: fundamental frequency and f_e: sampling frequency.

7. Simulation and Interpretation

The static and dynamic performances of IFOC strategy in the healthy and faulty state are evaluated using the MATLAB®/Simulink software. Several tests were carried out such as start-up with low-speed operation, rated load, and reverse test of speed.

7.1 Results for Healthy Machine

Figures 6(a) and 6(b) shows the motor speed and the stator currents under healthy conditions of the machine. The test of control is realised with an inversion of the speed direction from +20 [rad/s] to -20 [rad/s] at time t = 2s. This change of direction of rotation proceeds with the application of a load torque equal to 3.5N.m at time t=1s.

Despite the load variations, the speed follows the reference value, which proves the robustness of this technique even with variation or change of the speed rotation direction.

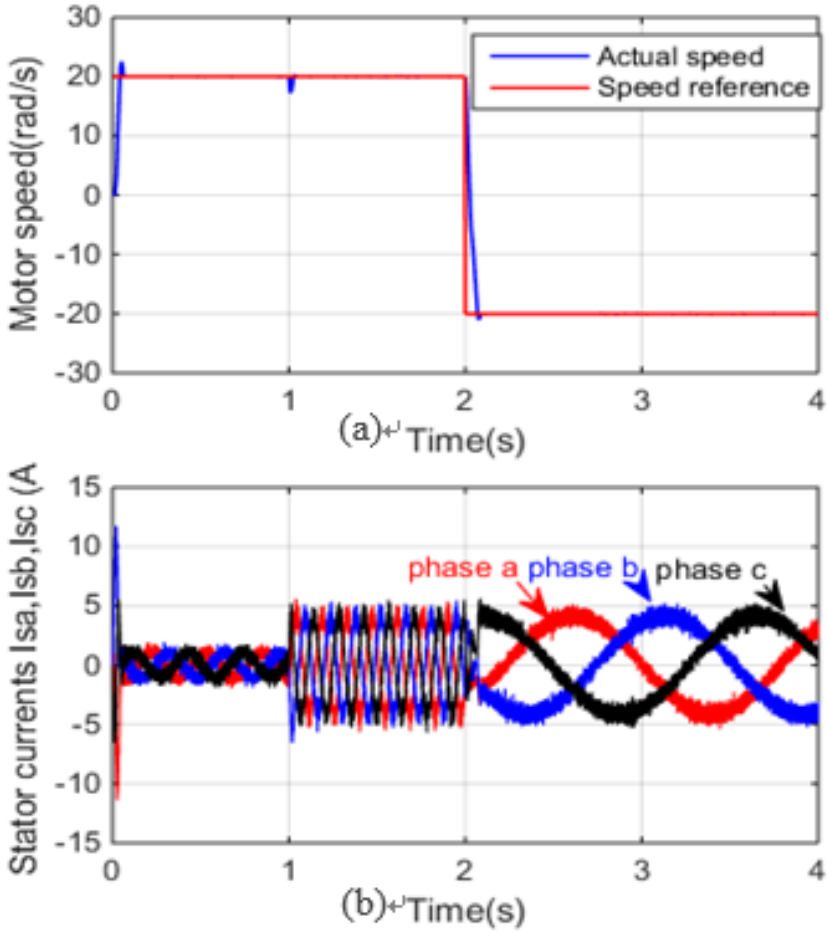

Fig. 6. Healthy condition of the motor: (a) Motor speed, (b) Stator Currents

7.2 Results for Machine with Mixed Eccentricity Fault

We applied a mixed eccentricity fault ME5% (SE=5% and DE=5%) and ME=10% (SE=10% and DE=10%) at start-up of motor. The figures 7(a-b) and 8(a-b) show the effects of these defects. Fig. 7(b) and 8(b) displays the evolution of the stator current; firstly we start with no load and then, at time t =1s, a load torque of 3.5[N.M] is applied with the mixed eccentricity fault. As

shown in these figures, a significant increase of the oscillations in stator current signals particularly between t = 1s and t = 4s are due to the present of the eccentricity defect component.

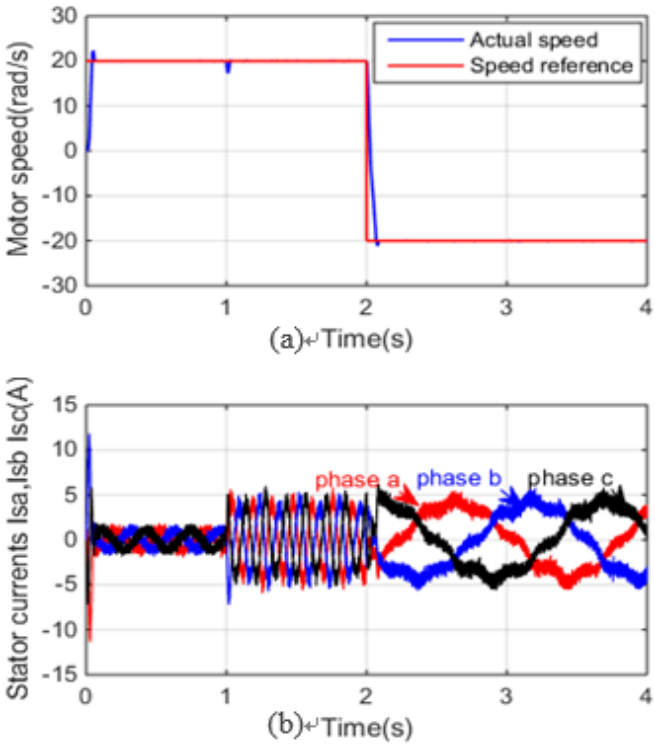

Fig. 7. Faulty motor with mixed eccentricity fault (ME 5%): (a) Motor speed, (b) Stator currents

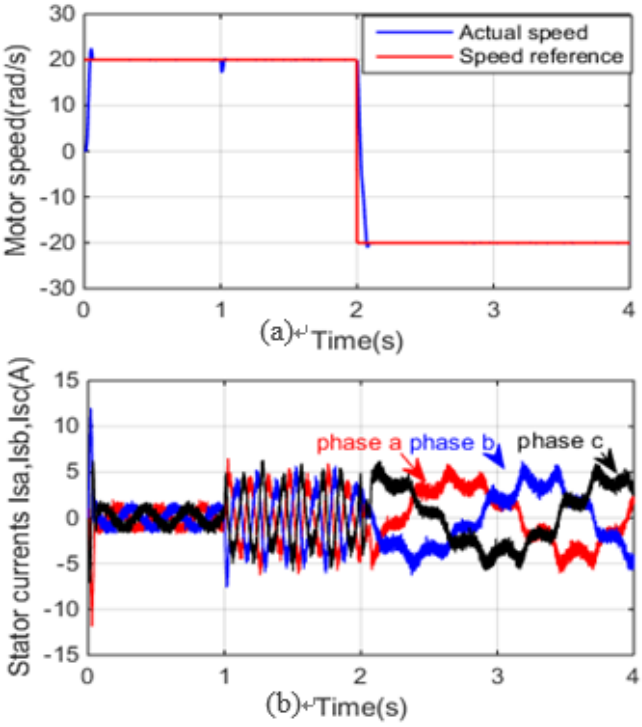

Fig. 8. Faulty motor with mixed eccentricity fault (ME 10%): (a) Motor speed, (b) Stator currents

In fig. 7(a) and 8(a) we observe that speed always remains stable and follows the reference the rotor speed follows the reference value without any significant oscillations; the application of mixed eccentricity fault and the load does not affect the rotor speed. These results show that the fuzzy logic speed controller is robust and presents a strong performance.

7.3 Current Park's Vector Analysis

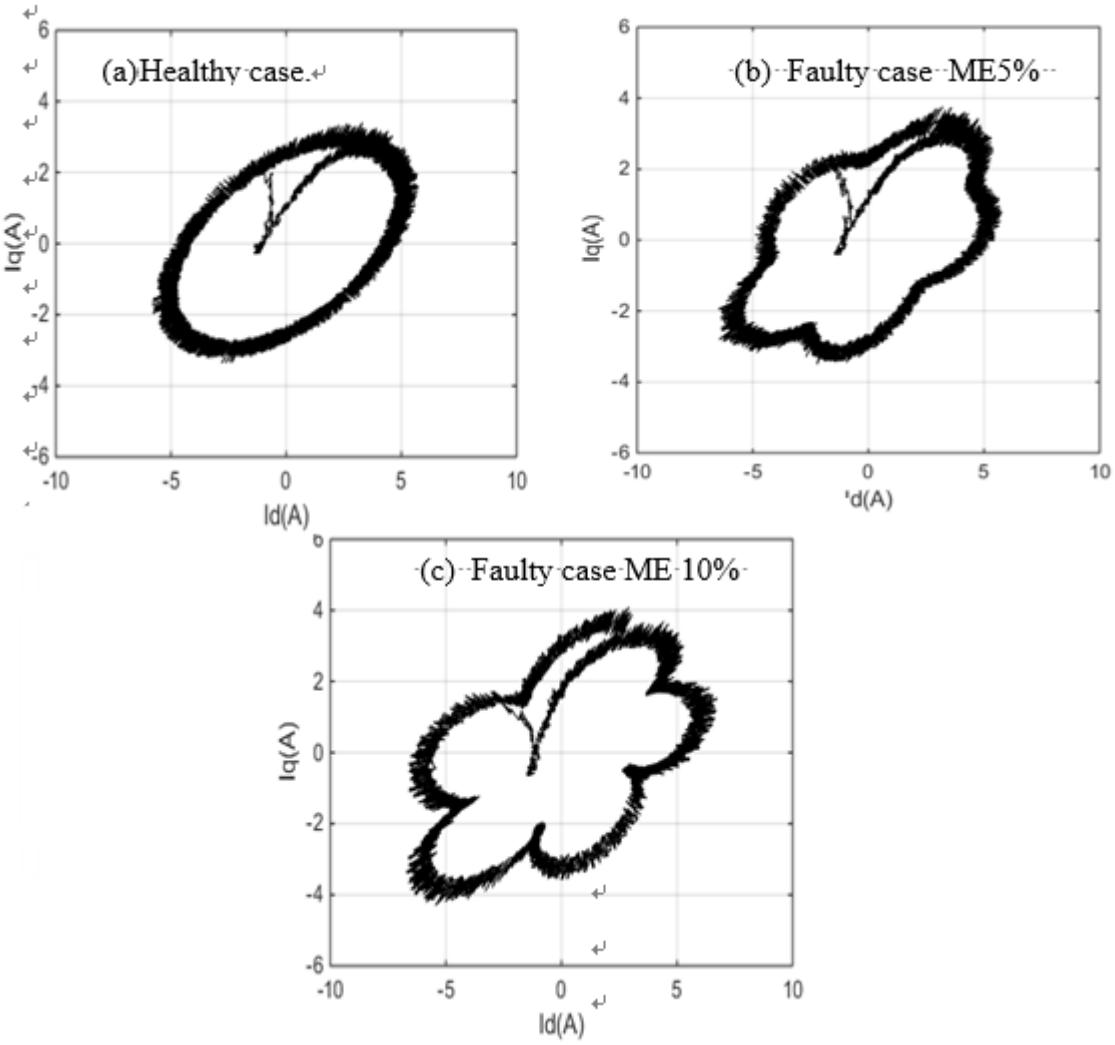

Fig. 9. Park's current vector approach for healthy and faulty machine

The figures 9(a-b-c) show the obtained 2-D Park's current vector for both healthy and mixed eccentricity fault cases. In the Fig. 9(a), the current pattern of park vector has an elliptic shape. However, in the case of eccentricity fault, the current pattern shape shown in fig. 9 (b-c) is totally different from the elliptic one, which indicates the eccentricity fault. It could be seen that current pattern for the faulty motor is clearly different from the current pattern of the healthy motor. This clearly shows the diagnosis capability of the Park's Vector approach. But this method alone can't give us specification on severity fault degree which is a paramount information, because we have

not to deal with all the eccentricity faults with the same manner. Therefore, we applied discrete wavelet transform which allows us to investigate and then appreciate this eccentricity fault sternness.

7.4 DWT analysis

The decomposition in multi-levels of the stator currents is carried out using the mother wavelet Daubechies44 (db44). The levels of necessary decomposition are calculated with the following relationship:

$$N = \text{int}\left[\frac{\log(\frac{f_e}{f_s})}{\log(2)}\right] + 2 = 12 \quad levels \tag{35}$$

In the case of our simulation, fundamental frequency (f_s = 7 Hz) is obtained directly by frequency analysis of the stator current, and sampling frequency (f_e = 10 kHz). So, the number of appropriate decompositions is equal to 12 levels. Table 2 indicates the different frequency bands of approximation and details.

Table 2. Frequency bands of approximation and details

Levels	Frequency bands approximation	Frequency bands details
7	0-39.0625	39.0625-78.125
8	0-19.531	19.531-39.0625
9	0-9.76	9.76_-19.531
10	0-4.88	4.88-9.76
11	0-2.44	2.44-4.88
12	0-1.22	1.22-2.44

Fig. 10, Fig11 and Fig 12, show the DWT analysis of the stator current signal given in Figs. 6.b-7b and 8.b (stator currents phase a). On the other hand, d12, d11, and d10 are the detail signals obtained by DWT decomposition with the mother wavelet db44 at level 12, in both healthy and faulty cases.

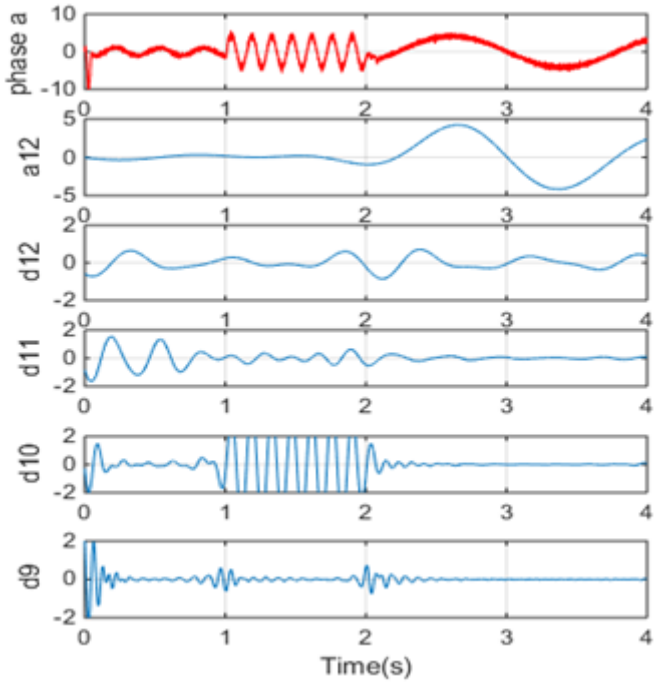

Fig. 10. DWT analysis of stator current for the healthy machine

A comparison between Figs 10-11 and fig 12, when we applied a load torque at t = 1s and changed the direction of rotation at t = 2s, indicates that in the d12 level signal, there is no much change but there are an important variation in the d10 and d11 level signals containing low band frequency caused by the harmonics of the eccentricity fault.

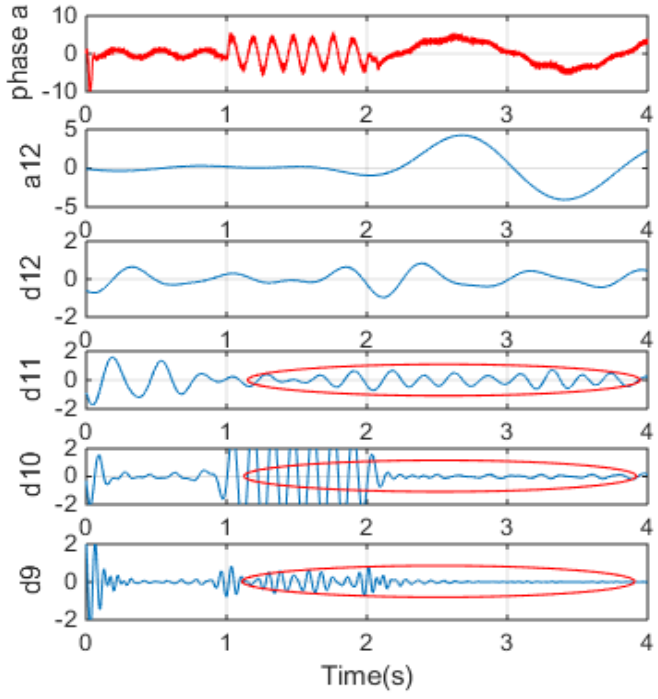

Fig. 11. DWT analysis of stator current for faulty machine under (ME 5%)

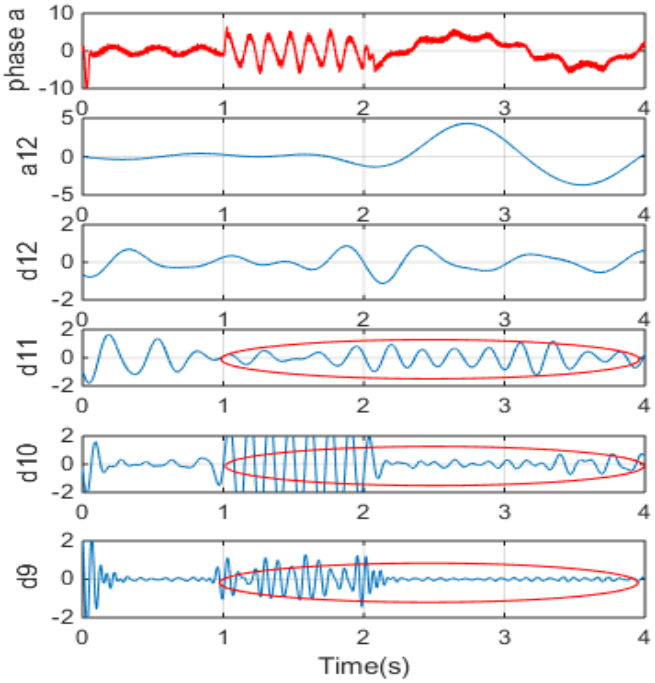

Fig. 12. DWT analysis of stator current for faulty machine under (ME 10%)

Fig. 13, shows the variation of the energy in the frequency bands of decomposition of multi wavelet-levels in the case of a healthy machine and with different degrees of mixed eccentricity defects: (ME1%,ME2%,ME 5%, ME 10%, ME15%,ME 20% and ME 25%).

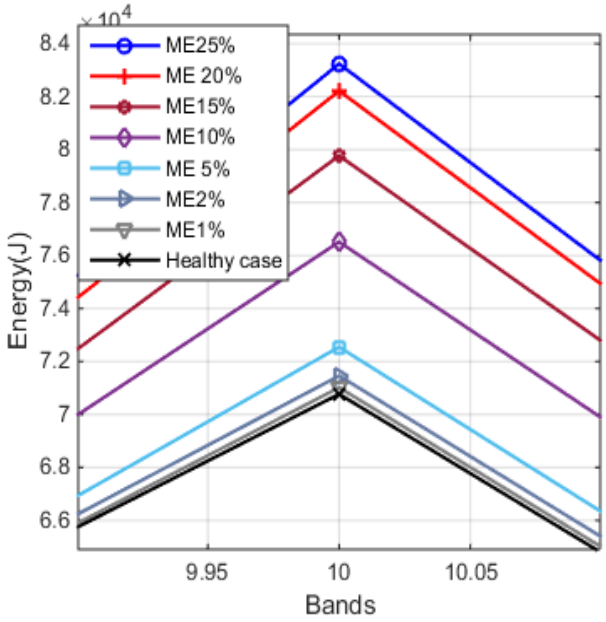

Fig. 13. Energy calculation from stator current for healthy and faulty cases

The stored energy in each level of decomposition, confirms the observed increase in the signals of detail and approximation especially in the level d10 and d11 (see Table 2).This is

corresponding to the band of neighborhood and below of the fundamental f_s=7HZ. The effect of the mixed eccentricity default is clearly manifested by the stored energy in the level 10.

The increase differs according to the severity of the default. It can be seen that the difference between the healthy and the faulty cases is very clear, and the increase of energy differs according to the severity of default.

Conclusions

The aim of this work is the diagnosis of air-gap mixed eccentricity fault in variable speed induction motor based on a robust fuzzy logic controller using two methods. The first method is based on the current park vector; the current pattern obtained gives a clear indication of the presence or not of eccentricity fault in comparison with the healthy case. The other complementary method is based on the discrete wavelet analysis and energy level. The simulation results of wavelet transformation give the advantageous information to decide the faulty situation, particularly in the presence of eccentricity fault. The results showed that the energy level increase simultaneously with the increasing degree of the eccentricity fault. However, the energy in healthy case always presents the lowest level.

Therefore, it is concluded that the employed technique can be used as a reliable tool for detection of the eccentricity fault as well as the evaluation of its severity degree.

Appendix

The machine parameters used in the simulation are listed in the table below:

Machine parameter	***Numerical value***
Output power	*Pn*=1.1 kW
Stator voltage	*Vs* =220 /380V
Stator frequency	*f* =50 Hz
Nominal current	*In* =4.5/2.6A
Nominal speed	Ωn =2850tr/mn
Pole number	*p* =1
Stator resistance	*Rs*=7.58 Ω
Rotor resistance	*Rr*=6.3 Ω
Rotor bar resistance	*Rb*=0.15 mΩ
Resistance of end ring segment	*Re*=0.15 mΩ

Rotor bar inductance	*Lb*=0.1 μH
Inductance of end ring	*Le*=0.1 μH
Leakage inductance of stator	*Lsf*=26.5mH
Mutual inductance	*Msr*=46.42 mH
Number of turns per stator	*Ns*=160
Number of rotor bars	*Nbr*=16

References

1. S. Chacko, C.N. Bhende, S. Jain, R.K. Nema, Modeling and simulation of field oriented control induction motor drive and influence of rotor resistance variations on its performance, 2016, Electrical and Electronics Engineering: An International Journal, vol. 5, no 1.
2. K. Hasse, Dynamic of adjustable speed drives with converter-fed squirrel cage induction motors, 1968, (Germany) Ph. D. Dissertation, Darmstadt, Technische.
3. F. Blaschke, The principle of field orientation as applied to the new transvector closed-loop control system for rotating-field machines, 1972, Siemens Rev, vol. 34, no. 3, pp. 217-220.
4. M. Akar, Detection of a static eccentricity fault in a closed loop driven induction motor by using the angular domain order tracking analysis method, 2013, Mechanical Systems and Signal Processing, vol. 34, no. 1-2, pp. 173-182.
5. H. Talhaoui, A. Menacer, A. Kessal, R. Kechida, Fast Fourier and discrete wavelet transforms applied to sensorless vector control induction motor for rotor bar faults diagnosis, 2014, ISA Transactions, vol. 53, no. 5, pp. 1639-1649.
6. T. Ameid, A. Menacer1, H. Talhaoui I. Harzelli1, Broken rotor bar fault diagnosis using fast Fourier transform applied to field-oriented control induction machine: simulation and experimental study, 2017, Int. J Adv Manuf. Technol., vol. 92, no. 1-4, pp. 917-928.
7. A. Chaouch, M. Harir, A. Bendiabdellah, P. Remus, Instantaneous Power Spectrum Analysis To Detect Mixed Eccentricity Fault In Saturated Squirrel Cage Induction Motor,*3rd* international Conference on Automation , Control, Engineering and Computer Science 2016.
8. I. Ouachtouk, S. Elhani, S. guedira, k. dahil, l Sadiki, Advanced Model of Squirrel Cage Induction Machine for Broken Rotor Bars Fault Using Multi Indicators, 2016, power engineering and electrical engineering, vol. 14, no. 5.
9. J.R. Magdaleno, H.P. Barreto, J.R. Cortes, R.M. Caporal, I.C.Vega, Vibration Analysis of Partially Damaged Rotor Bar in Induction Motor under Different Load Condition Using DWT , 2016, Hindawi Publishing Corporation, vol. 2016, ID 3530464.

10. B. Bessam, A. Menacer, M. Boumehraz, H. Cherif, Wavelet transform and neural network techniques for inter-turn short circuit diagnosis and location in induction motor, 2015, Int. J Syst Assur Eng Manag, vol. 8, pp. 478-488.
11. A. Jawadekar, S. Paraskar, S. Jadhav, G. Dhole, Artificial neural network-based induction motor fault classifier using continuous wavelet transform, 2014,Systems Science & Control Engineering, vol. 2, pp. 684–690 .
12. W. Laala, S-E. Zouzou, S.Guedidi, Induction motor broken rotor bars detection using fuzzy logic: experimental research, 2013, Int. J Syst Assur Eng Manag, vol. 5, no. 3, pp. 329–336.
13. El H. El Bouchikhi, V Choqueuse, M Benbouzid, Condition Monitoring of Induction Motors Based on Stator Currents Demodulation ,2015,International Review of Electrical engineering, vol. 10, no 6, pp. 704-715.
14. R. Kechida, A. Menacer, DWT Wavelet Transform for the Rotor Bars Faults Detection in Induction Motor, Electric Power and Energy Conversion Systems (EPECS), 2nd International Conference 2011.
15. K. Yahia, A.J.M. Cardoso, A. Ghoggal, S.E. Zouzou, Induction motors air-gap-eccentricity detection through the discrete wavelet transform of the apparent power signal under non-stationary operating, 2014, conditions, *ISA* Transactions, vol. 53(2), pp. 603-611.
16. N. Bessous, S. E. Zouzou, W. Bentrah, S. Sbaa, M. Sahraoui, Diagnosis of bearing defects in induction motors using discrete wavelet transform, Int. J Syst Assur Eng Manag, 2015 page 1.
17. Jawad Faiz and S.M.M. Moosavi, Eccentricity fault detection – From induction Machines to DFIG, A review Renewable and Sustainable Energy Reviews, 2016, vol. 55, no. c, pp. 169-179.
18. W. Wroński, M. Sułowicz, A. Dziechciarz, Dynamic and Static Eccentricity Detection in Induction Motors in Transient States, 2015, Technical Transactions Electrical Engineering, vol. 112, no. 2-E, pp. 171-194.
19. A. Intesar, A. Manzar, I. Kashif, M. Shuja Khan, Detection of Eccentricity Faults in Machine Using Frequency Spectrum Technique, February, 2011, International Journal of Computer and Electrical Engineering, vol. 3, no. 1.
20. N. Mehla, R. Dahiya, Detection of Bearing Faults of Induction Motor Using Park's Vector Approach ,2010, International Journal of Engineering and Technology, vol. 2(4), pp. 263-266.
21. C.da. Costa, M. Kashiwagi, M. H.Mathias, Rotor failure detection of induction motors by wavelet transform and Fourier transform in non-stationary condition, 2015, Case Studies in Mechanical Systems and Signal Processing, vol. 1, pp.15-26.

22. K. M. Siddiqui, K. Sahay, V.K. Giri.Early, Diagnosis of Bearing Fault in the Inverter Driven Induction Motor by Wavelet Transform , International Conference on Circuit, Power and Computing Technologies, 2016.